Combustion Dynamics of Plasma-Enhanced Premixed and Nonpremixed Flames

Xing Rao, Steve Hammack, Tonghun Lee, Campbell Carter, and Igor B. Matveev

***Abstract*—Combustion dynamics are investigated for plasma-enhanced methane–air flames in premixed and nonpremixed configurations using a transient arc dc plasmatron. Planar laser-induced fluorescence images of hydroxyl (OH) and carbon monoxide (CO) radicals are obtained over a range of equivalence ratios ($\phi = 0.7-1.3$), flow rates (6–18 LPM), and plasma powers (100–900 mA) to monitor radical propagation and *in situ* fuel reforming. The flow rates presented here are outside the range of normal flame stability. In the nonpremixed mode, the fuel is injected separately as a coflow around the plasma discharge, resulting in a unique two-cone flame front geometry, and the flame stability is mainly dependent on the flow dynamics. For premixed flames, partial oxidation occurs inside the chamber, resulting in higher energy conversion efficiencies, and stability is shown to be sensitive to the combustion chemistry. Both configurations are significantly influenced by *in situ* fuel reforming at higher plasma powers.**

***Index Terms*—Carbon monoxide, fuel reforming, hydroxyl, laser induced fluorescence, plasma assisted combustion, premixed and nonpremixed flame.**

I. Introduction

PLASMA-ASSISTED combustion, particularly that involving nonequilibrium discharges, is receiving much attention due to its potential for increased efficiency, extension of the flammability limit, reliable ignition in harsh operating conditions, integration of alternative fuels with variations in burning characteristics [1], [2], and for development of next-generation hypersonic propulsion systems [3], [4]. The exact mechanisms for flame enhancement by a plasma are still being actively studied, but a number of studies have provided insight into various aspects of this process [5]–[15]. Several pathways that have been identified as important in the way electromagnetic energy alters the reaction chemistry include the following: decomposition of the fuel from larger to smaller hydrocarbons and creation of radicals via collision with electrons; radiation-induced electron excitation; increased flame temperature by ohmic heating; and increase in excited state species, ions and electrons. Recently, the process of *in situ* fuel reformation, where the fuel is converted rapidly to syngas (mixture of CO and H_2), has also been proposed [10] as a key mechanism of enhanced flame stabilization. Kim *et al.* [16] found that H enhancement of hydrogen flame was not observed when hydrocarbon combustion was enhanced under the same condition, indicating the role of fuel reforming in PAC system. The reactions for *in situ* fuel reforming of methane are primarily carried out by $CH_4 + H_2O \rightarrow CO + 3H_2$, $C + CO_2 \rightarrow 2CO$, and $C + H_2O \rightarrow CO + H_2$ [17].

From a practical perspective, the geometry of the plasma discharge and the flame is also a critical parameter that influences both chemistry and the flow dynamics of the system, and prototype systems have displayed many variations. In this study, we investigate the impact of plasma on flame structure, chemical species production (OH and CO), and energy efficiency for premixed and nonpremixed flame configurations. A quasi nonequilibrium plasma discharge from a transient-arc dc plasmatron is used over a wide range of flow rates and input powers to stabilize a methane–air flame. The plasma and flame interaction can drastically change depending on the relative location of the reaction zone and discharge, resulting in varying degrees of thermal and nonequilibrium effects for combustion enhancement. By understanding the impact of the plasma discharge for these configurations, we can deduce optimized design guidelines for a new generation of practical plasma-enhanced combustion systems with higher efficiency and increased combustion stability.

II. Transient Arc DC Plasmatron (Premixed and Nonpremixed)

The discharge system used in this study is a transient arc dc plasmatron [18]–[21] from "Applied Plasma Technologies" and is shown in Fig. 1. The plasmatron exit has dimensions of 5 mm for the inner diameter, and the arc chamber is about 50 mm in length. This discharge system operates on a repetitive glow-to-spark transition mode, offering the advantages of a thermal plasmatron with low average power output, low average temperatures (600 K–1300 K), and high electron density. The torch operates primarily in the glow mode where high voltage ($\sim$10 kV) is applied between the cathode (inner electrode) and the surrounding anode. During the glow-to-spark transition, a short duration spark ($\sim$100 ns) [18] or diffuse channel arises and propagates toward the torch tip. As the overall temperature is low, however, the electrode erosion is significantly less than with traditional dc torches, and the torch can withstand prolonged operation without internal cooling.

Manuscript received August 17, 2010; revised September 20, 2010; accepted October 5, 2010. Date of current version December 10, 2010. This work was supported by AFOSR under reward FA9550-09-1-0282 and FA9550-10-1-0556.

X. Rao, S. Hammack, and T. Lee are with Michigan State University, East Lansing, MI 48824 USA.

C. Carter is with the Air Force Research Laboratory, Wright–Patterson AFB, OH 45433 USA.

I. B. Matveev is with Applied Plasma Technologies, McLean, VA 22101 USA.

Color versions of one or more of the figures in this paper are available online at http://ieeexplore.ieee.org.

Digital Object Identifier 10.1109/TPS.2010.2087041

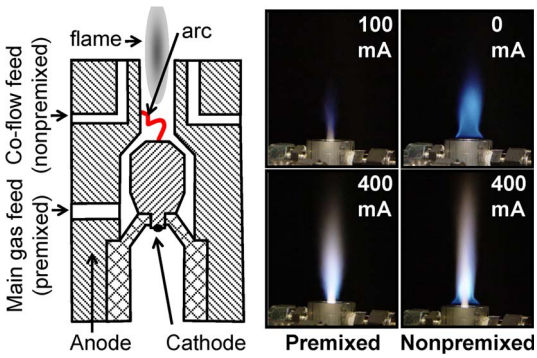

Fig. 1. (Left) Schematic of transient arc plasmatron with cathode in the center and two different inlets are used to get two different experimental setup. Images for premixed (100- and 400-mA dc currents) and nonpremixed (0 and 400-mA dc currents) flames of methane/air with equivalence ratio of 0.9.

There are two gas inlets in this discharge system: A lower one is connected directly to the arc chamber, and a top inlet provides coflow around the main exit of the torch, as shown in Fig. 1. In the premixed mode, a mixture of fuel and air flows through the lower inlet, while a nitrogen coflow is sent through the top inlet to further stabilize the flame and cut off entrainment of atmospheric oxygen. In the *nonpremixed mode*, air flows through the lower inlet (to generate the discharge), and methane through the top inlet. As this is an igniter for a combustor, it is designed for high flow with plasma stabilization. Therefore, most of the flow rates used in this study are conditions that are too high for unassisted stabilization; however, a few low-power nonpremixed mode settings where natural stabilization can be achieved are also employed, as shown in Fig. 1 (far right for the nonpremixed flames). Here, images for premixed (100- and 400-mA dc currents) and nonpremixed (0 and 400-mA dc currents) flames of CH_4–air are shown. It can be seen that, in both modes, the height of the illuminated region is increased with higher dc current due to the presence of a plasma plume. For premixed flames, the reaction mainly occurs inside the chamber at low dc currents, while at higher currents, the discharge plume is observed outside the torch as the plasma is not fully quenched inside the cavity. For nonpremixed flames, the combustion occurs entirely outside the chamber (since there is no fuel in the plasma chamber), and the center region shows a bright white hue as the plasma plume interacts with the flame. The anchor of the nonpremixed flame can be seen at the base of the plasma plume. Both the size and luminosity of the plume increase as a function of the input power. For premixed mode, we are aware of the fact that partial oxidation can, in some cases, happen inside the chamber, but it is still important and interesting to investigate flame structure and radical propagation for both modes, and in the discussion, we have this in considerations.

III. Results and Discussion

A. Impact on Flame Structure and Radical Concentration

In order to visualize the region of rapid radical propagation and the extent of the hot reaction zone, hydroxyl (OH) radical imaging was carried out. UV laser radiation near 283 nm

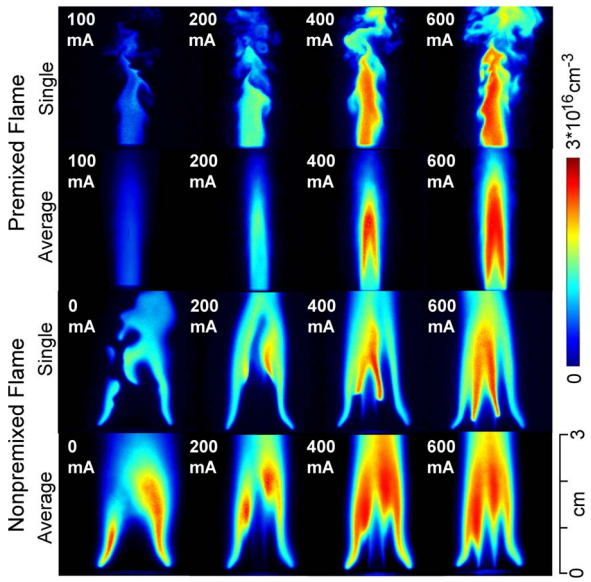

Fig. 2. Single and averaged 2-D OH PLIF images as a function of increasing microwave power for both (top) premixed flames and (bottom) nonpremixed flames.

was used for planar laser-induced fluorescence (PLIF) of OH using the $Q_1(8)$ transition from $A^2\Sigma^+ - X^2\Pi$ (1, 0) [22]. A Lumonics Hyperdye HD-300 dye laser, pumped by a Q-switched Nd:YAG laser, was used for generating 566-nm radiation. The 566-nm beam was doubled in frequency through an Inrad Autotracker (ATIII) to a final output frequency of 283 nm with linewidth of ~ 0.1 cm^{-1}. The 283.029-nm laser was expanded into a sheet using a two-lens telescope, and the fluorescence signal was collected using an intensified CCD camera with a Schott WG-305 filter for suppression of the Rayleigh and surface scattering. It should be noted that the ground state population of the $N_1 = 8$ state is relatively insensitive to temperatures in the range of 1200 K–2300 K: The peak Boltzmann population fraction occurs near 1600 K and has decreased by less than 10% at 1200 K and 2300 K. We also note that, due to the small size of this flame, absorption (of the laser beam) and fluorescence trapping are not expected to be significant.

Single and ensemble averaged OH PLIF images are shown in Fig. 2 as a function of increasing microwave power for both premixed (top) and nonpremixed flames (bottom). Average images were based on the acquisition of 200 instantaneous images. Here, the total flow rate for the reactants is 9 standard liters per minute (SLPM) (referenced to STP conditions), and the equivalence ratio is $\phi = 0.95$. The equivalence ratio in the nonpremixed case is defined here as the ratio between the fuel and oxygen in the inner nozzle. At these conditions, combustion power from the oxidation of the fuel is about $\sim$500 W using the lower heating value of methane. For first-order comparisons showing rough magnitude and trend, measurements using a thermocouple show that temperatures for premixed flames are about 100 K–200 K higher than that in nonpremixed flames for the same fuel flow rates. For premixed flames, the visible flame luminosity and plasma volume increase with increased current/power. The range for current is 100–900 mA in our

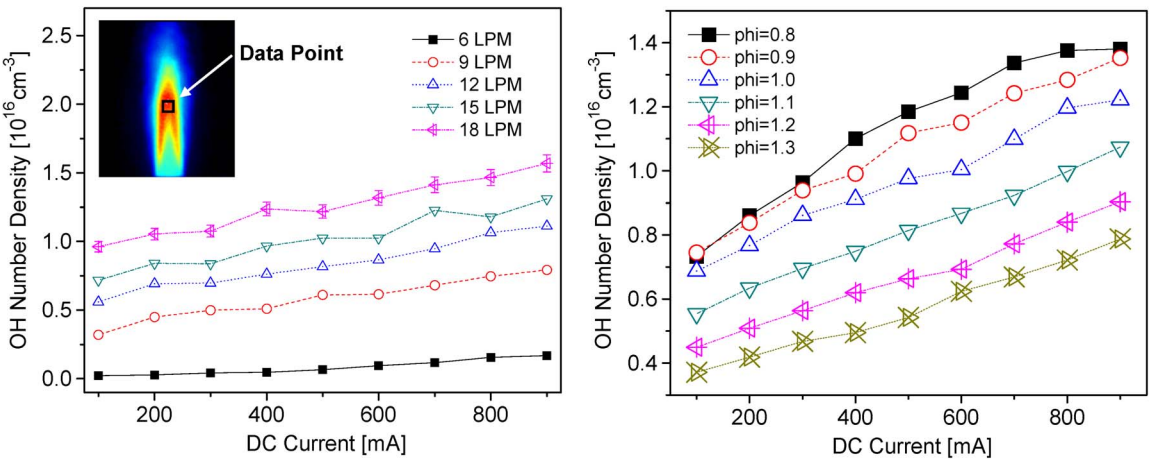

Fig. 3. OH number density is plotted for different dc currents, total flow rates (left, equivalence ratio is fixed at 0.95 and for different dc current), and equivalence ratios (right, total flow rate is fixed at 15 LPM) in premixed mode.

current research, resulting a discharge power of 150–750 W. At low powers (∼100 mA), the OH signal is lower than in a typical premixed flame, presumably because a significant portion of the oxidation reactions occur inside the arc chamber, where the mixture initially comes in contact with the discharge. When the dc current is higher, the reaction rates are expected to increase, resulting in a more compact flame structure particularly as a larger portion of the fuel is oxidized inside the chamber. However, the introduction of added species and charged particles with more momentum (and new reaction chemistry involving ions and electrons) gives rise to new chemical pathways, which ultimately results in a higher concentration of OH radicals, such as $O(^3P) + H_2O \rightarrow OH + OH$ and $O(^1D) + H_2O \rightarrow OH + OH$ [23]. The sources of $O(^3P)$ and $O(^1D)$ are believed to be mainly from $O_2 + e \rightarrow O(^3P) + O(^1D) + e$ [24], which often involves the Herzberg and Schumann-Runge systems of the O_2 molecule.

As can be seen in Fig. 2, nonpremixed flames show a unique two-cone flame structure: Within the inner cone, the main oxidation of the fuel with the air from the plasma discharge takes place; within the outer cone, combustion with the ambient air also occurs. Overall, the height of the flame is larger for the nonpremixed mode than for the premixed case, while the flow appears to be more turbulent in the premixed flames due to the shorter reaction zone than in the subsequent nonpremixed flames with the ambient air. As previously stated, the outer cone flame in the nonpremixed mode can be sustained without any dc plasma power input for some of the lower flow rates used in this study. In the nonpremixed flame, the reaction zone of the outer cone remains relatively constant as power is increased. However, the inner cone is dramatically increased as highly reactive air interacts with the fuel. At powers exceeding 400 mA, the OH LIF intensity for the inner flame front is much higher than that for the outer one, and the flame stability is dominated by the plasma discharge.

The number density of the OH was calibrated from the LIF signal using a Hencken Burner with a near-stoichiometric methane–air mixture in the weakly excited fluorescence regime of OH. The uncertainty of the resulting OH number densities is estimated as ±20% of the indicated value. This accounts for the uncertainty of the calibration number density (from the original absorption measurements) and for the application of the calibration to these flames (accounting for differences in quenching rates, temperatures, laser sheet intensity, etc.). In Fig. 3, the OH number density is plotted for different dc currents, total flow rates, and equivalence ratios for the premixed mode. In the left portion of Fig. 3, the equivalence ratio is fixed, while the dc current and the total flow rate are changed. The data points are taken at a fixed height in the center of the reaction zone (shown in the inset) where OH LIF is most intense. For low total flow rates (6 LPM), the flow is not strong enough to propagate the nanosecond arc discharge to the end of the plasmatron chamber, and most of the fuel is partially oxidized inside the chamber, resulting in a low OH concentration above the tip. It is clear that, with higher dc currents (higher dc power), the OH number density increases almost linearly with the input power. For different total flow rates, it is noticeable that all the OH number densities at 100 mA are less than 10^{16} cm^{-3}, which is the typical OH production level in a Bunsen flame without plasma enhancement. This is an indication that the plasma is mostly acting to dissociate and preheat the fuel inside the arc chamber and combustion outside is generally not influenced by the discharge itself. It can be seen from Fig. 3 (right side) that OH is highest with an equivalence ratio of 0.8 and is less at values of 0.9 and 1.0 [25], [26]. This is due to the fact that OH production is, in this case, a combination of direct coupling of the mixture inside the chamber and partial coupling after exiting the torch, and higher OH concentration in lean conditions indicates that the oxidation of lean mixtures extends further out to the tip. The increase of OH number density with dc power levels is a direct influence of the plasma chemistry such as additional oxidation of product water vapor (H_2O) by electron impact. H_2O plays an active role in the production of active radicals through direct electron impact disassociation, i.e., $e + H_2O \rightarrow H + OH + e$, and reaction with $O(^1D)$ disassociated from O_2, i.e., $O(^1D) + H_2O \rightarrow 2OH$ and $e + O_2 \rightarrow O(^1D) + O(^3P) + e$ [27]. These radicals, in turn, result in increased OH production which can offset termination

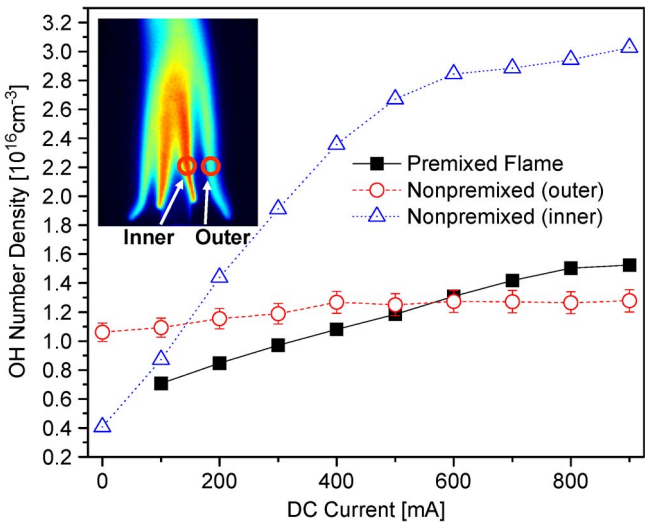

Fig. 4. OH number density with the same flow conditions (total flow rate is 9 SLPM, and $\phi = 0.95$) but different currents for both premixed (from data point, the same as in Fig. 3) and nonpremixed (two data points, one is the outer flame front and the other is the inner flame front) flames.

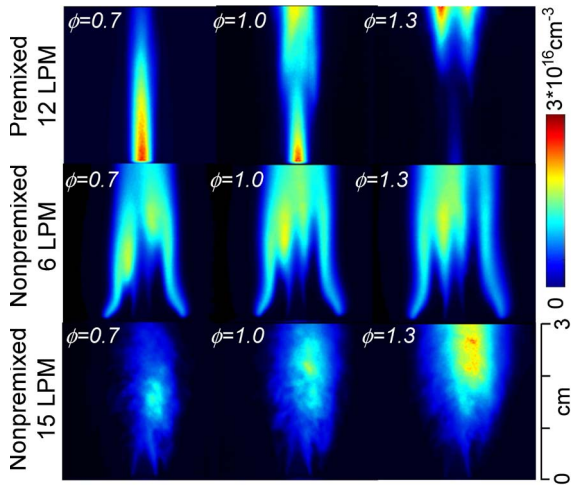

Fig. 5. (Top) Averaged OH PLF images for all flow rates at premixed mode with $\phi = 0.7, 1.0$, and 1.3. Averaged OH PLF images for (middle) 6 LPM and (bottom) 15 LPM at nonpremixed mode with $\phi = 0.7,\ 1.0,$ and 1.3.

reactions when the dc power is higher. If the power is further increased, we anticipate that OH production pathways will be saturated and reach a plateau.

A first-order comparison of OH densities for both premixed and nonpremixed flames is shown in Fig. 4. In this plot, the OH number densities are shown at the same flow rates, but with increasing levels of power input for both flame geometries. For the premixed flame, the data are extracted from a central location identical to that shown in Fig. 3. For the nonpremixed flame, the data are extracted from two locations, representing the inner and outer cones, as shown in the inset of Fig. 4.

The OH number density in the premixed mode increases by almost 100% from 100 to 900 mA of dc current input. In contrast for nonpremixed flames, the OH number density remains relatively stable on the outer flame front and is close to the Burner flame OH production rates, which indicates that the outer flame has little influence from the inside air discharge. However, the OH number density in the inner flame front shows an increase close to 750%, and the highest OH number density reaches over 3×10^{16} cm^{-3}, which is more than twice that of the OH production of premixed flame at the exact same condition. This shows that much of the flame enhancement for the nonpremixed mode is carried out at the inner flame front as the power is enhanced. For the inner flame, the significant increase in OH number density comes from the active excited species in the air discharge exiting the plasma chamber, including atomic oxygen, which has been previously documented as a significant factor for flame enhancement [8] and a cause for increase in concentration of OH. A Chemkin simulation using GRI-mech 3.0 [28] with a premixed burner model of flame with methane and air shows that, with the addition of 10^{-4} mole fraction of atomic oxygen, the OH number density increases by about 40%. This increase is lower than the increase in both premixed mode and inner flame of diffusion mode indicating other pathways for OH increase.

B. Flame Stability, CO Formation, and Energy Efficiency

The influence of geometry and other parameters on the flame stability can also be observed from the OH PLIF images. Fig. 5 shows averaged OH PLF images for both premixed and nonpremixed flames at various flow rates and equivalence ratios. The top row shows a premixed flame with a rate of 12 SLPM, with equivalence ratios of $\phi = 0.7,\ 1.0,$ and 1.3. The bottom two rows show a nonpremixed mode flow rates of 6 SLPM (middle)/15 SLPM (bottom) with overall equivalence ratios of $\phi = 0.7,\ 1.0,$ and 1.3. In the premixed mode, the figures represented here are generally reproduced for all the flow rates where the flame is stable at the end of the plasmatron tip for leaner conditions; however, the flame tends to lift off at higher equivalence ratios ($\phi = 1.3$, top row in Fig. 5). At high equivalence ratios, the radical pool is poorly established, and the fuel/air mixture tends to react more with ambient air, resulting in combustion downstream of the exit. Nonpremixed flames at low flow rates (6 SLPM, middle row in Fig. 5) do not reflect this phenomenon, and the flame is stable over a wide range of equivalence ratios. For higher total flow rates (15 SLPM, bottom row in Fig. 5), the stability of the nonpremixed flame is compromised; the outer flame is no longer visible in the turbulent structure, and the two flame zones merge into a single structure. The stability for these two configurations is different in that the premixed mode appears to be more chemistry driven and dependent on the equivalence ratio and the nonpremixed mode is more dependent on the flow rates and the physical interaction of the fuel and the plasma discharge itself. Overall, the premixed mode can stabilize higher flow rates, but the smaller dimensions of the combustion and sensitivity on the fuel and air ratios can render the premixed mode more difficult to use.

The CO number density is measured using two-photon-absorption LIF to investigate the *in situ* fuel reforming into carbon monoxide (CO) and hydrogen (H_2), which is believed to be a key mechanism for flame stabilization [10]. CO was measured with two-photon PLIF, using the $B^1\Sigma^+ - X^1\Sigma^+$ (0, 0) transition at 230.10 nm [29]. A Sirah Precisionscan LG-2400

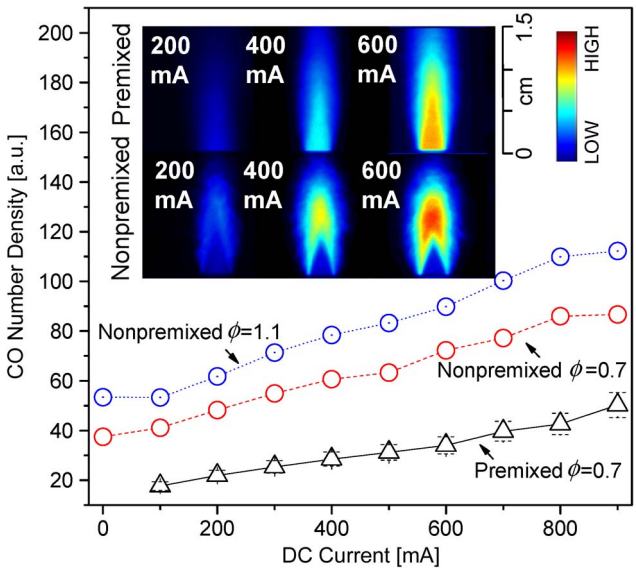

Fig. 6. Averaged CO PLF images for (inset, top) premixed and (inset, bottom) nonpremixed. CO number density is plotted with equivalence ratios of 0.7 (premixed and nonpremixed) and 1.1 (nonpremixed).

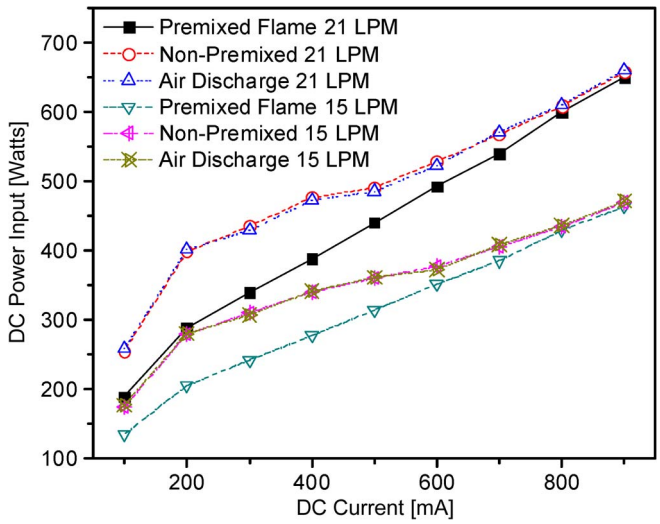

Fig. 7. DC power input with different current for air plasma, premixed flames, and nonpremixed flames.

dye laser was pumped by a 532-nm beam from a Q-switched Nd:YAG laser. The 653-nm output of the dye laser was sum-frequency-mixed with the third harmonic beam (355 nm) from the injection seeded Nd:YAG laser to produce 18 mJ/pulse of 230-nm radiation (linewidth of ~ 0.1 cm^{-1}). CO fluorescence is then detected at 486 nm using an intensified CCD camera fitted with an interference filter (10-nm FWHM). In Fig. 6, averaged CO PLF images for premixed (inset, top row) and nonpremixed (inset, bottom row) are shown, and CO PLIF intensity is plotted for both modes with equivalence ratios of $\phi = 0.7$ and 1.1. Due to the two-photon excitation of the CO, the quality of the LIF signal for the nonlinear process is not as high as that of OH and, coupled with a more diffused profile of CO, did not resolve the two cones of the nonpremixed flame. It should be noted that, because of the weak absorption, the laser sheet is smaller and more focused near the center; therefore, a dramatic drop of CO downstream is an artifact of the laser sheet.

In the lower portion of Fig. 6, the CO PLIF signal intensity is corrected for the quadratic dependence [30] on the laser power to reproduce a relative CO number density (a.u.), as the irradiance is not high enough for photoionization to exceed quenching, in our case, to influence the quadratic dependence [31]. We can assume that an increase of CO in the reaction zone is indicative of *in situ* fuel reforming which leads to a temporary increase in hydrogen (H_2). The H_2 to CO connection is only valid for the reaction zone region and not reflected in the overall byproduct as conversion to H_2O and CO_2 occurs. For both modes, CO LIF intensity is shown to increase with increased dc current input. It is clear that, for nonpremixed and premixed flames, CO LIF intensity for rich flames $(\phi = 1.1)$ is higher than that for lean flames $(\phi = 0.7)$. Comparison between CO number densities between premixed and nonpremixed flames at equivalence ratio of 0.7 indicates that higher fuel reforming is observed for the nonpremixed flame over the entire range of powers used in this study. This is expected as a very rich interface is established in the nonpremixed flame between the plasma discharge and the fuel. For both flame configurations, we see a gradual rise in CO as power is increased. This additional CO generated from the *in situ* reforming of the fuel will contribute as a major mechanism for flame stabilization by increasing the hydrogen content of the mixture. We have to assume that CO increase also indicates temporary increase of hydrogen. Increase of CO is about 30 a.u. in the premixed flame and 40–50 a.u. in the nonpremixed mode for the same condition over the power range from 0 to 800 mA.

For plasma-assisted combustion, energy consumption (the energy needed for the same amount of air with the same current can be used to show energy efficiency here) during the coupling process is a critical parameter. Fig. 7 shows the actual input power as a function of input current under identical flow conditions. It is clear that most power is required for the air-only plasma as significant energy is required for dissociation, ionization, and vibration excitation of nitrogen, resulting in significant NO_x generation [21]. When combustion is present, the breakup of the nitrogen is assisted by the exothermic reactions involving the fuel, and ionization threshold itself is lowered. Therefore, the conversion efficiency to H_2 and CO is subsequently increased. In the premixed mode at lower dc currents, power consumption is lower as fuel is injected into the discharge chamber, and *in situ* breakup of CH_4 molecules and plasma impact reactions further accelerate the reaction chemistry. At higher dc current, however, the power consumption for premixed and nonpremixed flames is seen to converge as plasma impact reactions and fuel breakup are eventually saturated for both configurations.

IV. Conclusion

A dc plasmatron characterized by a nanosecond glow-to-arc transient has been used to investigate premixed and nonpremixed flames using OH LIF and CO two-photon-absorption LIF. A unique two-cone flame geometry for the nonpremixed mode, where the inner cone produced by the plasma enhanced air mainly interacting with the flame. Partial oxidation inside

the chamber for premixed flames here consumed less dc power thus had higher energy efficiencies. For nonpremixed flames, the flame is mainly stabilized by the reactive discharge of air in the inner core, and the stability of nonpremixed flames is significantly influenced by the flow rates of the gases. By comparison of OH PLIF images in both modes for different total flow rates and equivalence ration, stability of premixed flames is more dependent on chemistry. The OH number density for the inner and outer cones indicates the increase of OH with increased discharge power, while stability for nonpremixed case depends on the inner cone from discharge. Two photon LIF measurements of relative CO number density showed that CO number density increases with high discharge power, indicating that both configurations are significantly influenced by *in situ* fuel reforming at higher plasma powers. In the future, we will work on simulations with detailed discharge and combustion interaction mechanisms and figure out important reaction pathways.

ACKNOWLEDGMENT

The authors would like to thank Dr. J. Tishkoff as the Technical Monitor.

REFERENCES

[1] S. M. Starikovskaia, "Plasma assisted ignition and combustion," *J. Phys. D, Appl. Phys.*, vol. 39, no. 16, pp. R265–R299, Aug. 2006.

[2] A. Y. Starikovskii, "Plasma supported combustion," *Proc. Combust. Inst.*, vol. 30, no. 2, pp. 2405–2417, Jan. 2005.

[3] A. B. Leonov, D. A. Yarantsev, A. P. Napartovich, and I. V. Kochetov, "Plasma-assisted ignition and flameholding in high-speed flow," presented at the 44th AIAA Aerospace Sciences Meeting, Reno, NV, 2006, Paper AIAA-2006-563.

[4] S. B. Leonov and D. A. Yarantsev, "Plasma-induced ignition and plasma-assisted combustion in high-speed flow," *Plasma Sources Sci. Technol.*, vol. 16, no. 1, pp. 132–138, Feb. 2007.

[5] X. Rao, K. Hemawan, I. Wichman, C. Carter, T. Grotjohn, J. Asmussen, and T. Lee, "Combustion dynamics for energetically enhanced flames using direct microwave energy coupling," *Proc. Combust. Inst.*, 2010, to be published.

[6] W. Sun, M. Uddi, T. Ombrello, S. Won, C. Carter, and Y. Ju, "Effects of non-equilibrium plasma discharge on counterflow diffusion flame extinction," *Proc. Combust. Inst.*, 2010, to be published.

[7] T. Ombrello, Y. Ju, and A. Fridman, "Kinetic ignition enhancement of diffusion flames by nonequilibrium magnetic gliding arc plasma," *AIAA J.*, vol. 46, no. 10, pp. 2424–2433, 2008.

[8] T. Ombrello, S. H. Won, and Y. Ju, "Lifted flame speed enhancement by plasma excitation of oxygen," presented at the 47th AIAA Aerospace Sciences Meeting Exhib., Orlando, FL, 2009, Paper AIAA-2009-689.

[9] W. Kim, H. Do, M. G. Mungal, and M. A. Cappelli, "Plasma-discharge stabilization of jet diffusion flames," *IEEE Trans. Plasma Sci.*, vol. 34, no. 6, pp. 2545–2551, Dec. 2006.

[10] W. Kim, M. Godfrey Mungal, and M. A. Cappelli, "The role of in situ reforming in plasma enhanced ultra lean premixed methane/air flames," *Combust. Flame*, vol. 157, no. 2, pp. 374–383, Feb. 2009. DOI: 10.1016/j.combustflame.2009.06.016.

[11] E. Mintusov, A. Serdyuchenko, I. Choi, W. R. Lempert, and I. V. Adamovich, "Mechanism of plasma assisted oxidation and ignition of ethylene-air flows by a repetitively pulsed nanosecond discharge," presented at the 46th AIAA Aerospace Sciences Meeting Exhib., Reno, NV, 2008, Paper AIAA 2008-1106.

[12] M. Uddi, N. Jiang, E. Mintusov, I. V. Adamovich, and W. R. Lempert, "Atomic oxygen measurements in air and air/fuel nanosecond pulse discharges by two photon laser induced fluorescence," presented at the 46th AIAA Aerospace Sciences Meeting Exhib., Orlando, FL, 2008, Paper AIAA 2008-1110.

[13] E. S. Stockman, S. H. Zaidi, R. B. Miles, C. D. Carter, and M. D. Ryan, "Measurements of combustion properties in a microwave enhanced flame," *Combust. Flame*, vol. 156, no. 7, pp. 1453–1461, Jul. 2009.

[14] K. W. Hemawan, C. L. Romel, S. Zuo, I. S. Wichman, T. A. Grotjohn, and J. Asmussen, "Microwave plasma-assisted premixed flame combustion," *Appl. Phys. Lett.*, vol. 89, no. 14, p. 141 501, Oct. 2006.

[15] K. W. Hemawan, I. S. Wichman, T. Lee, T. A. Grotjohn, and J. Asmussen, "Compact microwave re-entrant cavity applicator for plasma-assisted combustion," *Rev. Sci. Instrum.*, vol. 80, no. 5, p. 053 507, May 2009.

[16] W. Kim, H. Do, M. G. Mungal, and M. A. Cappelli, "A study of plasma-stabilized diffusion flames at elevated ambient temperatures," *IEEE Trans. Plasma Sci.*, vol. 36, no. 6, pp. 2898–3004, Dec. 2008.

[17] E. Achenbach and E. Riensche, "Methane/steam reforming kinetics for solid oxide fuel cells," *J. Power Sources*, vol. 52, no. 2, pp. 283–288, Dec. 1994.

[18] Y. D. Korolev, O. B. Frants, N. V. Landl, V. G. Geyman, and I. B. Matveev, "Glow-to-spark transitions in a plasma system for ignition and combustion control," *IEEE Trans. Plasma Sci.*, vol. 35, no. 6, pp. 1651–1657, Dec. 2007.

[19] Y. D. Korolev, O. B. Frants, N. V. Landl, V. G. Geyman, and I. B. Matveev, "Nonsteady-state gas-discharge processes in plasmatron for combustion sustaining and hydrocarbon decomposition," *IEEE Trans. Plasma Sci.*, vol. 37, no. 4, pp. 586–592, Apr. 2009.

[20] Y. D. Korolev and I. B. Matveev, "Nonsteady-state processes in a plasma pilot for ignition and flame control," *IEEE Trans. Plasma Sci.*, vol. 34, no. 6, pp. 2507–2513, Dec. 2006.

[21] X. Rao, I. Matveev, and T. Lee, "Nitric oxide formation in a premixed flame with high-level plasma energy coupling," *IEEE Trans. Plasma Sci.*, vol. 37, no. 12, pp. 2303–2313, Dec. 2009.

[22] K. Kohse-Hoinghaus and J. B. Jeffries, *Applied Combustion Diagnostics*. New York: Taylor & Francis, 2002.

[23] R. Ono and T. Oda, "OH radical measurement in a pulsed arc discharge plasma observed by a LIF method," *IEEE Trans. Ind. Appl.*, vol. 37, no. 3, pp. 709–714, May/Jun. 2001.

[24] B. Eliasson, M. Hirth, and U. Kogelschatz, "Ozone synthesis from oxygen in dielectric barrier discharges," *J. Phys. D, Appl. Phys.*, vol. 20, no. 11, p. 1421, 1986.

[25] Y. Ju, S. O. Macheret, M. N. Shneider, R. B. Miles, and D. J. Sullivan, "Numerical study of the effect of microwave discharge on the premixed methane-air flame," presented at the 40th AIAA/ASME/SAE/ASEE Joint Propulsion Conf. Exhib., Fort Lauderdale, FL, 2004, Paper AIAA 2004-3707.

[26] Q. V. Nguyen, R. W. Dibble, C. D. Carter, G. J. Fiechtner, and R. S. Barlow, "Raman-LIF measurements of temperature, major species, OH, and NO in a methane-air bunsen flame," *Combust. Flame*, vol. 105, no. 4, pp. 499–510, Jun. 1996.

[27] J. J. Lowke and R. Morrow, "Theoretical analysis of removal of oxides of sulphur and nitrogen in pulsed operation of electrostatic precipitators," *IEEE Trans. Plasma Sci.*, vol. 23, no. 4, pp. 661–671, Aug. 1995.

[28] GRI-Mech 3.0. [Online]. Available: http://www.me.berkeley.edu/gri-mech/version30

[29] J. M. Seitzman, J. Haumann, and R. K. Hanson, "Quantitative two-photon LIF imaging of carbon monoxide in combustion gases," *Appl. Opt.*, vol. 26, no. 14, pp. 2892–2899, Jul. 1987.

[30] J. B. Kelman, D. A. Greanhalgh, E. Ramsay, D. Xiao, and D. T. Reid, "Flow imaging by use of femtosecond-laser-induced two-photon fluorescence," *Opt. Lett.*, vol. 29, no. 16, pp. 1973–1975, Aug. 2004.

[31] A. V. Mokhov, H. B. Levinsky, C. E. V. D. Meij, and R. A. A. M. Jacobs, "Analysis of laser-induced-fluorescence carbon monoxide measurements in turbulent nonpremixed flames," *Appl. Opt.*, vol. 34, no. 30, pp. 7074–7082, Oct. 1995.

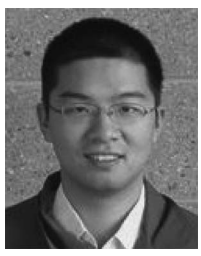

Xing Rao was born in Jinxi, China, on March 26, 1985. He received the B.S. degree in mechanical engineering and the M.S. degree in nuclear engineering from Tsinghua University, Beijing, China, in 2005 and 2007, respectively, and the Ph.D. degree in mechanical engineering from Michigan State University, East Lansing, in 2010.

He is currently a Postdoctoral Fellow with Michigan State University. His research interests include laser diagnostics in plasma-assisted combustion and energetic-nanoparticle-enhanced combustion.

Dr. Rao is a member of the American Institute of Aeronautics and Astronautics and the Combustion Institute.

Steve Hammack was born in Chicago, IL, on May 13, 1988. He received the B.S. degree in mechanical engineering from Michigan State University, East Lansing, in 2009, where he is currently working toward the Ph.D. degree.

He is currently a Graduate Research Assistant with Michigan State University. His research interests include laser diagnostics of combustion and plasma-assisted combustion.

Mr. Hammack is a Student Member of the American Institute of Aeronautics and Astronautics.

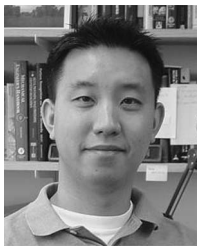

Tonghun Lee was born in Seoul, Korea, on April 3, 1974. He received the B.S. degree in mechanical engineering from Yonsei University, Seoul, Korea, in 2000 and the M.S. and Ph.D. degrees in mechanical engineering from Stanford University, Stanford, CA, in 2002 and 2006, respectively.

He is currently an Assistant Professor with the Department of Mechanical Engineering, Michigan State University, East Lansing. His research interests include laser diagnostics of high-pressure combustion systems, plasma-enhanced flames, and oxidation of novel biofuels. His research group at Michigan State University is devoted to fundamental research in applying laser-based optical methods for development of advanced combustion and propulsion system technologies.

Campbell Carter was born in Refugio, TX, in 1958. He received the B.S. degree in mechanical engineering from the University of Texas, Austin, and the Ph.D. degree in mechanical engineering from Purdue University, West Lafayette, IN.

Upon leaving Purdue, he joined the Combustion Research Facility, Sandia National Laboratories, as a Postdoctoral Fellow, where he worked with Dr. Robert Barlow on making simultaneous measurements of major and minor combustion species in turbulent flames. He joined Systems Research Laboratories in 1993 and then Innovative Scientific Solutions, Inc., in 1997, developing and applying laser diagnostic techniques for the advanced propulsion group at the U.S. Air Force Research Laboratory (AFRL), Wright–Patterson AFB, OH. Since 2002, he has worked directly for AFRL. His area of focus has been the development and application of advanced laser diagnostics to harsh flow fields.

Dr. Carter is an Active Member of the combustion and combustion diagnostics communities. He is a Fellow of the American Society of Mechanical Engineering and an Associate Fellow of the American Institute of Aeronautics and Astronautics.

Igor B. Matveev was born in Samara, Russia, on February 11, 1954. He received the M.S. and Ph.D. degrees in mechanical engineering from the Nikolaev Shipbuilding Institute, Nikolaev, Ukraine, in 1977 and 1984, respectively. His Ph.D. thesis was entitled "Development and implementation of the plasma ignition systems for naval gas turbines."

From 1977 to 1990, he was a Researcher, a Teacher, and an Associate Professor with the Nikolaev Shipbuilding Institute. In 1990, he established Plasmatechnika Ltd., a privately owned company for the development and mass production of plasma systems. Since 2003, he has been with Applied Plasma Technologies, McLean, VA, where he is the President and CEO. His current research interests are focused on novel PAC technologies and on the creation of international research teams for their development and implementation.